Advanced Composite Materials
Publication details, including instructions for authors and subscription information:
http://www.tandfonline.com/loi/tacm20

Thermal deformation constraint using response surfaces for optimization of stacking sequences of composite laminates

Akira Todoroki [a], Takumi Ozawa [a], Yoshihiro Mizutani [a] & Yoshiro Suzuki [a]

[a] Department of Mechanical Sciences and Engineering, Tokyo Institute of Technology, 2-12-1 Ookayama, Meguro, Tokyo, 1528552, Japan

Published online: 04 Jun 2013.

To cite this article: Akira Todoroki, Takumi Ozawa, Yoshihiro Mizutani & Yoshiro Suzuki (2013) Thermal deformation constraint using response surfaces for optimization of stacking sequences of composite laminates, Advanced Composite Materials, 22:4, 265-279, DOI: 10.1080/09243046.2013.805502

To link to this article: http://dx.doi.org/10.1080/09243046.2013.805502

Advanced Composite Materials, 2013
Vol. 22, No. 4, 265–279, http://dx.doi.org/10.1080/09243046.2013.805502

Thermal deformation constraint using response surfaces for optimization of stacking sequences of composite laminates

Akira Todoroki*, Takumi Ozawa, Yoshihiro Mizutani and Yoshiro Suzuki

Department of Mechanical Sciences and Engineering, Tokyo Institute of Technology, 2-12-1 Ookayama, Meguro, Tokyo 1528552, Japan

(*Received 13 March 2013; accepted 13 May 2013*)

Carbon fiber reinforced plastic (CFRP) laminates are used extensively in aerospace structures. The laminated CFRP composite structures require optimal design of the stacking sequences. Modifications to the stacking sequences change the thermal deformation that results from the CFRP laminate curing process. Even if a stacking sequence provides maximum buckling load, the laminate is unacceptable if it displays large deformations after the curing process. Therefore, this study deals with the constraint of thermal deformation after the curing process. Maximization of the buckling load was targeted as the objective function here. Three types of response surfaces were proposed to estimate the thermal deformation and their fit was investigated. The mode classification method was found to be excellent. Using the mode classification response surface, a stacking sequence optimization to maximize the buckling stress was performed. The new mode classification method was shown to be appropriate for optimization of the curing process constraints.

Keywords: buckling; laminates; thermal deformation; optimization

1. Introduction

Carbon fiber reinforced plastic (CFRP) laminates are used extensively in aerospace structures and their applicability for automobile structures in the next generation electric vehicles is now being investigated. As the laminated CFRP composites have strong anisotropic properties, the CFRP composite structures require optimal design of the stacking sequences and component dimensions. Miki [1] and Fukunaga [2] both proposed a graphical optimization method using the lamination parameters. For practical laminated CFRP structures, however, the available fiber angles are limited to a small set of angles, 0°, 45°, −45°, and 90°, because of the lack of experimental data on the building block approach to aircraft design. This causes combinatorial optimization of the fiber angles of CFRP laminates.

To optimize the stacking sequence of laminated CFRP composites, genetic algorithms (GAs) have been adopted in many research programs.[3–11] Narita proposed a layer-wise optimization method for the stacking sequence design.[12]

Our research group has proposed a fractal branch and bound (FBB) method for optimizing the stacking sequence of laminated CFRP composites.[13,14]. This method

*Corresponding author. Email: atodorok@ginza.mes.titech.ac.jp

employs a quadratic polynomial for the response surface using lamination parameters, such as the buckling load, to approximate the objective functions. This method has low computational cost and a practical optimal result can be obtained by the deterministic process in milliseconds. The FBB method is based on the discovery that plots of the feasible laminates create fractal patterns in the lamination-parameter space. Since, this method is one of branch and bound approaches, tuning of the parameters is not required. This method has been applied successfully to the problem of maximizing the buckling load of a laminate [15] and of the flutter limit [16] with constraints.

For a practical stiffened panel made from laminated CFRP structures, the dimensions of the stiffener and panel must be optimized simultaneously, in addition to optimizing the stacking sequence. Researchers have published papers that deal with the modified efficient global optimization method using multi-objective GAs (MOGA). [17,18] In addition, a constraint to prevent fracturing is dealt with using Kriging response surfaces.[19]

The efficient global optimization method using MOGA [17] is an excellent method for optimizing stiffened composite panels. The method uses two-level optimizations: at the first level, dimensions of the stiffened CFRP laminate are optimized and at the second, the stacking sequence at given dimensions of the stiffened CFRP laminate is optimized. The stacking sequence optimizations of the CFRP laminates at the given dimensions are, therefore, one of the important issues for optimizing composite structures.

Modifications of the stacking sequences cause changes in CFRP laminate stiffness (changes in buckling load, vibration mode, and deflection). Modifications of the stacking sequence change the thermal deformation caused during the curing of CFRP laminates, because the linear thermal expansion coefficients and elastic modulus are changed. Even if a stacking sequence provides maximum buckling load, the laminate is unacceptable when the laminate deforms extensively after the curing process. Thermal deformation is not dealt with as a constraint in previous optimization processes, because it is complex. In this study, therefore, the constraint of thermal deformation is dealt with. As an objective function, buckling load maximization is adopted here. First of all, linear thermal expansion coefficients are investigated using lamination parameters. Three types of response surfaces using quadratic polynomials are used in this study, to evaluate the constraint at low computational cost: a response surface using lamination parameters, a response surface using lamination parameters and thermal expansion coefficient, and a response surface with thermal deformation classification. As thermal deformation is dealt with as a constraint in this study, an entire search algorithm is adopted to find an optimal result to prevent differences in optimizer performance. The performance of the three types of the response surfaces are investigated here.

2. Lamination parameters and linear thermal expansion coefficients

In this section, the two types of lamination parameters, in-plane (V) and out-of-plane (W), are explained briefly.

The in-plane stiffness terms of the symmetric laminates are represented with in-plane lamination parameters V_i^* as follows.

$$\begin{bmatrix} A_{11} \\ A_{22} \\ A_{12} \\ A_{66} \\ A_{16} \\ A_{26} \end{bmatrix} = h \begin{bmatrix} U_1 & V_1^* & V_2^* \\ U_1 & -V_1^* & V_2^* \\ U_4 & 0 & -V_2^* \\ U_5 & 0 & -V_2^* \\ 0 & \frac{1}{2}V_3^* & V_4^* \\ 0 & \frac{1}{2}V_3^* & -V_4^* \end{bmatrix} \begin{bmatrix} 1 \\ U_2 \\ U_3 \end{bmatrix} \tag{1}$$

where h is the thickness of the laminate, U_i ($i=1,...,5$) are the material invariants, and V_i^* ($i=1,...,4$) are the in-plane lamination parameters. The material invariants are given as follows.

$$\begin{aligned} U_1 &= \tfrac{1}{8}(3Q_{11} + 3Q_{22} + 2Q_{12} + 4Q_{66}) \\ U_2 &= \tfrac{1}{2}(Q_{11} - Q_{22}) \\ U_3 &= \tfrac{1}{8}(Q_{11} + Q_{22} - 2Q_{12} - 4Q_{66}) \\ U_4 &= \tfrac{1}{8}(Q_{11} + Q_{22} + 6Q_{12} - 4Q_{66}) \end{aligned} \tag{2}$$

where

$$\begin{aligned} Q_{11} &= \frac{E_L}{1 - v_{LT}v_{TL}}, \qquad Q_{22} = \frac{E_T}{1 - v_{12}v_{21}}, \\ Q_{12} &= \frac{v_{TL}E_T}{1 - v_{LT}v_{TL}}, \qquad Q_{66} = G_{LT} \end{aligned} \tag{3}$$

The in-plane lamination parameters are given as:

$$\mathbf{V} = \begin{bmatrix} V_1^* \\ V_2^* \\ V_3^* \\ V_4^* \end{bmatrix} = \frac{2}{h}\int_0^{h/2} \begin{bmatrix} \cos 2\theta \\ \cos 4\theta \\ \sin 2\theta \\ \sin 4\theta \end{bmatrix} dz \tag{4}$$

where z is the coordinate of the thickness direction, the origin is located in the middle of the plate, and $\theta(z)$ is the fiber angle of the location of z.

The out-of-plane stiffness terms of the laminates are represented with out-of-plane lamination parameters, W_i^*, as:

$$\begin{bmatrix} D_{11} \\ D_{22} \\ D_{12} \\ D_{66} \\ D_{16} \\ D_{26} \end{bmatrix} = \frac{h^3}{12} \begin{bmatrix} U_1 & W_1^* & W_2^* \\ U_1 & -W_1^* & W_2^* \\ U_4 & 0 & -W_2^* \\ U_5 & 0 & -W_2^* \\ 0 & \frac{1}{2}W_3^* & W_4^* \\ 0 & \frac{1}{2}W_3^* & -W_4^* \end{bmatrix} \begin{bmatrix} 1 \\ U_2 \\ U_3 \end{bmatrix} \tag{5}$$

The out-of-plane lamination parameters are defined as:

$$\mathbf{W} = \begin{bmatrix} W_1^* \\ W_2^* \\ W_3^* \\ W_4^* \end{bmatrix} = \frac{24}{h^3}\int_0^{h/2} z^2 \begin{bmatrix} \cos 2\theta(z) \\ \cos 4\theta(z) \\ \sin 2\theta(z) \\ \sin 4\theta(z) \end{bmatrix} dz \tag{6}$$

When the available fiber angles are limited to 0°, 90°, and ± 45°, sin4θ is always zero, which means that V_4^* and are always zero. When the angle plies of ±45° are balanced, the total sum of sin2θ is equal to zero. This means is always zero. When the ±45° plies are placed within a small distance, becomes very small: usually the value is negligible.

First, we consider the single ply linear thermal expansion coefficient of symmetric laminates. The thermal strains of fiber ε_L^T and transverse direction ε_T^T can be expressed as:

$$\varepsilon_L^T = \alpha_L \Delta T, \quad \varepsilon_T^T = \alpha_T \Delta T \tag{7}$$

where α_L is the linear thermal expansion coefficient of the fiber direction (L) and α_T is the linear thermal expansion coefficient of the transverse direction (T).

When the coordinate (x–y) of the strain is rotated by θ from the L–T coordinate, the thermal strain can be transformed as follows:

$$\begin{Bmatrix} \varepsilon_x^T \\ \varepsilon_y^T \\ \gamma_{xy}^T \end{Bmatrix} = \begin{bmatrix} \cos^2\theta & \sin^2\theta & 0 \\ \sin^2\theta & \cos^2\theta & 0 \\ 2\sin\theta\cos\theta & -2\sin\theta\cos\theta & 0 \end{bmatrix} \begin{Bmatrix} \varepsilon_L^T \\ \varepsilon_T^T \\ 0 \end{Bmatrix} \tag{8}$$

For the composite laminate, the elastic deformation strain vector ε^{N} can be expressed as:

$$\varepsilon^N = \varepsilon^{0N} + z\kappa^N \tag{9}$$

where ε^{0N} is the strain vector at the middle plane of the symmetric laminated composite plate and the κ is the curvature vector of the plate. The residual strain vector ε^R of the thermal deformation of each ply can be expressed as:

$$\varepsilon^R = \varepsilon^N - \varepsilon^T \tag{10}$$

where ε^T is the thermal strain vector at each ply.

Therefore, the residual stress of the kth ply can be written as:

$$\begin{Bmatrix} \sigma_x^R \\ \sigma_y^R \\ \tau_{xy}^R \end{Bmatrix}_{(k)} = \begin{bmatrix} \overline{Q}_{11} & \overline{Q}_{12} & \overline{Q}_{16} \\ \overline{Q}_{12} & \overline{Q}_{22} & \overline{Q}_{26} \\ \overline{Q}_{16} & \overline{Q}_{26} & \overline{Q}_{66} \end{bmatrix}_{(k)} \begin{Bmatrix} \varepsilon_x^R \\ \varepsilon_y^R \\ \gamma_{xy}^R \end{Bmatrix}_{(k)} \tag{11}$$

where $[\overline{\mathbf{Q}}]$ is the stiffness matrix of the angle ply.

As the external load is not applied here, the total sum of the stress must be balanced:

$$\int_{-h/2}^{h/2} \sigma_x^R dz = 0, \quad \int_{-h/2}^{h/2} \sigma_y^R dz = 0, \quad \int_{-h/2}^{h/2} \tau_{xy}^R dz = 0 \tag{12}$$

where h is the thickness of the laminated plate.

From Equations (10)–(12), the following relationship is obtained:

$$[\mathbf{A}]\begin{Bmatrix}\varepsilon_x^{0N}\\ \varepsilon_y^{0N}\\ \gamma_{xy}^{0N}\end{Bmatrix}=\int_{-h/2}^{h/2}[\overline{\mathbf{Q}}]\begin{Bmatrix}\varepsilon_x^{T}\\ \varepsilon_y^{T}\\ \gamma_{xy}^{T}\end{Bmatrix}dz \tag{13}$$

The linear thermal expansion coefficient of the laminated plate can be defined as:

$$\begin{Bmatrix}\overline{\alpha}_x\\ \overline{\alpha}_y\\ \overline{\alpha}_{xy}\end{Bmatrix}=\Delta T^{-1}\begin{Bmatrix}\varepsilon_x^{0N}\\ \varepsilon_y^{0N}\\ \gamma_{xy}^{0N}\end{Bmatrix} \tag{14}$$

From Equations (13) and (14), the linear thermal expansion coefficient of the laminated plate is obtained as:

$$\begin{Bmatrix}\overline{\alpha}_x\\ \overline{\alpha}_y\\ \overline{\alpha}_{xy}\end{Bmatrix}=[\mathbf{A}]^{-1}\int_{-h/2}^{h/2}[\overline{\mathbf{Q}}]\begin{Bmatrix}\alpha_L\cos^2\theta+\alpha_T\sin^2\theta\\ \alpha_L\sin^2\theta+\alpha_T\cos^2\theta\\ 2(\alpha_L-\alpha_T)\cos\theta\sin\theta\end{Bmatrix}dz \tag{15}$$

From Equation (15), each linear thermal expansion coefficient can be calculated:

$$\overline{\alpha}_x=\frac{V_1^*(K_2U_2-K_1U_2+K_2U_4)-V_1^{*2}K_2U_2+2K_1U_3V_2+K_1(U_1-U_4)}{2\{2V_2^*U_3(U_4+U_1)-V_1^{*2}U_2^{*2}+(U_1^2-U_4^2)\}} \tag{16}$$

$$\overline{\alpha}_y=-\frac{V_1^*(K_2U_1-K_1U_2+K_2U_4)+V_1^{*2}K_2U_2-2K_1U_3V_2-K_1(U_1-U_4)}{2\{2V_2^*U_3(U_4+U_1)-V_1^{*2}U_2^{*2}+(U_1^2-U_4^2)\}} \tag{17}$$

$$\overline{\alpha}_{xy}=-\frac{2V_2^*K_3}{(U_1-U_4)-2V_2^*U_3} \tag{18}$$

where K_1, K_2, and K_3 are the material invariants:

$$\begin{aligned}K_1&=(U_1+U_4)(\alpha_L+\alpha_T)+U_2(\alpha_L-\alpha_T)\\ K_2&=U_2(\alpha_L+\alpha_T)+(U_1+2U_3-U_4)(\alpha_L-\alpha_T)\\ K_3&=U_2(\alpha_L+\alpha_T)+2(U_3+U_5)(\alpha_L-\alpha_T)\end{aligned} \tag{19}$$

3. Optimization problem

In this study, a blade-stiffened composite plate (250 mm long, 160 mm wide, 16 mm high, 1 mm thick, 34.5 mm blade flange width, and 3.75 mm blade thickness) was selected as an optimization target (Figure 1). As the ply thickness of the laminate is 0.125, the total number of plates and blades are 8 and 30, respectively. The dimensions of the stiffened panel were the optimal values obtained in a previous paper.[20] The material was carbon/epoxy composite with properties listed in Table 1.

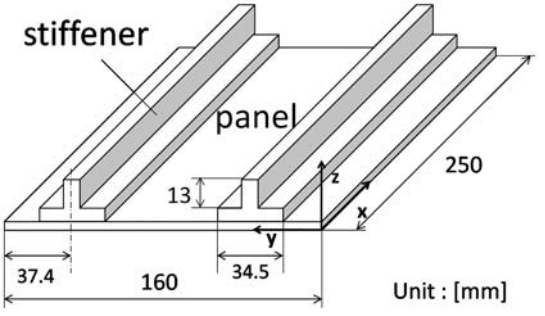

Figure 1. Blade-stiffened composite plate.

Table 1. Material properties.

E_L	E_T	E_Z	G_{LT}	G_{LZ}	G_{TZ} (Gpa)
141	10	10	5	5	0.15
ν_{LT}	ν_{LZ}	ν_{TZ}			
0.3	0.3	0.4			
α_L		α_T		α_Z (K^{-1})	
0.9×10^{-6}		30×10^{-6}		30×10^{-6}	

For the optimization, fiber angles were limited to the small set, 0°, 45°, −45°, and 90°, because of lack of experimental data. The number of +45°-ply and −45°-ply must be balanced according to the balance rule. According to the 4-ply rule, to prevent large matrix cracking, the same-fiber-angle ply must not exceed four plies.

The objective function of the stacking sequence optimization is the maximization of the buckling load. As a constraint, the thermal deformation of the plate warp is limited to 0.15 mm after curing. To obtain the buckling load and thermal deformation, commercially available FEM code ANSYS ver.12.0 was used with a 3-D solid of 20 nodes (solid 226).

For FEM analyses of the buckling stress, a uniform compression stress of 1 MPa was applied at both ends of the plate as a reference stress in the longitudinal direction. A linear buckling analysis method was adopted here to obtain minimum buckling stress. For the buckling analyses, the total number of nodes was 36,887 and total number of elements 18,944.

For the thermal deformation analyses, the center point of the composite panel was fixed. The temperature difference caused by curing is $\Delta T = -228$ °C. For the deformation, the maximum warp deformation was used as a constraint.

The stacking sequences of the plate and blade stiffener were design variables. The objective function was the response surface of the buckling stress. Maximization of the objective function with the thermal deformation constraint was the optimization problem. The thermal deformation was evaluated using the response surface of thermal deformation and maximum deformation of 0.15 mm. To aid the performance of the optimizer and to determine the exact performance of the response surface, an entire search of every laminate was adopted in the optimization because the evaluation cost was negligible for calculations of the response surfaces.

4. Response surface of thermal deformation

4.1. Lamination parameters

The response surface of the buckling stress was made using the lamination parameters in reference.[13–15,17,18] In a similar way, the response surface of the thermal deformation was also made from the lamination parameters. As shown in Equations (17)–(19), the linear thermal expansion coefficients were calculated using the lamination parameters when the composite material was fixed. The method was termed 'lamination-parameter response surface.'

In this study, quadratic polynomials were adopted for both response surfaces. As the number of lamination parameters is four per laminate, V_1^*, V_2^*, W_1^*, and W_2^*, the total number of variables was eight because there are two laminates (the plate and blade). The lamination parameters of the plate and stiffeners were expressed as V_1^{*P}, V_2^{*P}, W_1^{*P}, and W_2^{*P} and V_1^{*S}, V_2^{*S}, W_1^{*S}, and W_2^{*S}, respectively. When these eight parameters were used as variables in the quadratic polynomial, 35 unknown coefficients ($1+8+8+8\times 7/2=35$) had to be decided using the least-square-error method. For this response surface, V_1^{*P}, V_2^{*P}, W_1^{*P}, W_2^{*P}, V_1^{*S}, V_2^{*S}, W_1^{*S}, and W_2^{*S} were the variables. To obtain appropriate results, D-optimal laminates were selected as the design of experiments was performed.[21] One hundred laminates were selected and FEM analyses performed to obtain the buckling stress and thermal deformation. Using the FEM results, the response surfaces of the buckling stress and thermal stress were made. The fitness of the response surface was compared using the adjusted coefficients of determination (R^2_{adj}).

4.2. Thermal expansion coefficients

As shown in Equations (16)–(18), the linear thermal expansions of the composite laminate were not expressed as a linear function of the lamination parameters, but rather as rational functions. This implies that the thermal deformation response may not be expressed as a simple quadratic polynomial of lamination parameters. To express the rational functions, a higher order polynomial may be required. This indicates a significant increase in total number of unknown coefficients. To prevent the significant increase in unknown coefficients, linear thermal expansion coefficients were added as variables of the response surface of the quadratic polynomial. This means that V_1^{*P}, V_2^{*P}, W_1^{*P}, W_2^{*P}, V_1^{*S}, V_2^{*S}, W_1^{*S}, W_2^{*S}, α_x^{-P}, α_y^{-P}, α_{xy}^{-P}, α_x^{-S}, α_y^{-S}, and α_{xy}^{-S} are the variables of the response surface of the thermal deformation. Similarly, D-optimal laminates were selected in the design of experiments. Two hundred and fifty laminates were selected and FEM analyses performed to obtain the buckling stress and thermal deformation. Using the FEM results, the response surfaces of the thermal stress were made. The fitness of the response surface was compared using the adjusted coefficients of determination (R^2_{adj}). The method was termed the 'thermal coefficient response surface.'

4.3. Mode classification response surface

To obtain a more precise response surface of the thermal deformation, than the thermal coefficient response surface, a mode classification method was adopted. Many FEM analyses were performed to determine the modes of thermal deformation. Three kinds of modes of thermal deformation were observed: a saddle, simple extension, and non-symmetric type. The saddle type can be classified into two sub-types, A and B. These thermal deformation modes are shown in Figures 2 and 3.

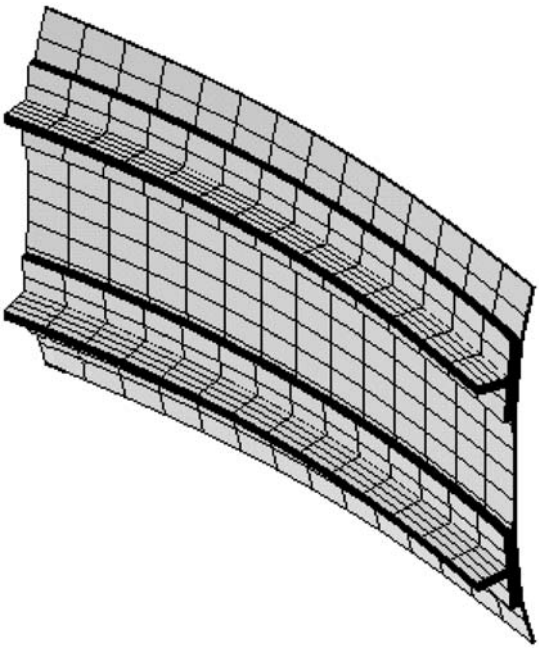

Figure 2. Saddle type A deformation.

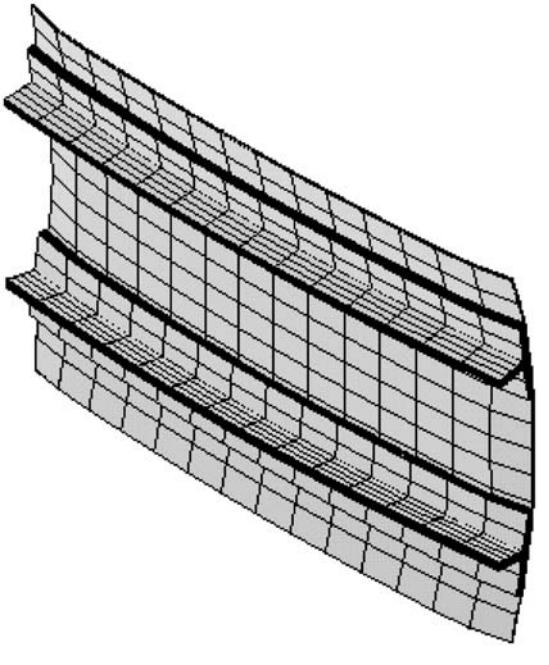

Figure 3. Saddle type B deformation.

We consider the case where the x- and y-coordinates are the longitudinal and transverse directions of the laminated plate, respectively. When $\alpha_x^{-P} < \alpha_x^{-S}$ and $\alpha_y^{-P} > \alpha_Y^{-S}$ are satisfied, the deformation mode is a type A saddle. When $\alpha_x^{-P} > \alpha_x^{-S}$ and $\alpha_y^{-P} < \alpha_Y^{-S}$ are

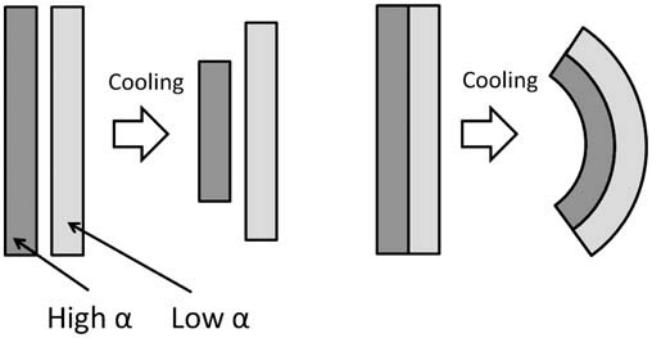

Figure 4. Schematic thermal deformation of stiffened composite plate.

satisfied, the deformation mode is a type B saddle. When $\alpha_x^{-P} = \alpha_x^{-S}$ and $\alpha_y^{-P} = \alpha_Y^{-S}$ are satisfied, the deformation mode is a simple extension type because both the plate and stiffener deform similarly. In the special case that the plate has many +45°-plies and −45°-plies, the deformation mode is of the twisting type. This is because the large values of W_3^* are not zero, although the W_3^* is very small for balanced laminates. This brings about coupling between the bending and twisting caused by D_{16} and D_{26}.

It can be concluded that the small difference in linear thermal expansion coefficients of the plate and stiffener are warped easily. Thus, the simple extension mode is neglected in this study. Moreover, W_3^* usually becomes very small for thick balanced CFRP laminates. This indicates that the twisting mode can be neglected for the actual balanced thick CFRP laminates. In this study, therefore, the saddle types A and B were selected as typical thermal deformation modes.

A schematic thermal deformation is shown in Figure 4. We consider the case where, the linear thermal expansion coefficient of the plate is larger than that of the stiffener. As a cooling process, the part with larger linear thermal expansion coefficient shrinks more. This means that the plate is the inner and the stiffener is the outer part, causing a warped saddle-like configuration. The difference in linear thermal expansion coefficients of the plate and stiffener causes a difference in thermal deformation modes. For the actual composite laminates, the higher thermal expansion coefficient in the x-direction equal to a lower one in the y-direction. This means that we can classify the thermal deformation mode by comparing α_x^{-P} and α_x^{-S}. After classification of the thermal deformation mode, two types of response surfaces were made using the lamination parameters and linear thermal expansion coefficients of the plate and stiffener. This means that V_1^{*P}, V_2^{*P}, W_1^{*P}, W_2^{*P}, V_1^{*S}, V_2^{*S}, W_1^{*S}, W_2^{*S}, α_x^{-P}, α_y^{-P}, α_{xy}^{-P}, α_x^{-S}, α_Y^{-S}, and α_{xy}^{-S} are variables of the response surface of the thermal deformation. In this method, two response surfaces were made to predict the thermal deformation of the laminated CFRP. As it is impossible to apply the simple D-optimal laminate design of experiments in this method, D-optimal laminates were selected from the set of candidate types A and B. Two hundred and 50 laminates were selected for each response surface.

5. Results and discussion

5.1. Comparison of response surfaces

The buckling stress response surface can be made easily using the lamination parameters.[13–15,17,18] The quadratic polynomial is sufficient for the buckling stress

response surface. Figure 5 shows estimation results of the response surface of the buckling stress. The abscissa is the buckling stress obtained by FEM analyses and the ordinate is the estimated result obtained by the quadratic polynomial response surface. The obtained adjusted coefficient of determination R^2_{adj} is 0.99. This means that the quadratic polynomial is sufficient for the response surface of the buckling stress as found in previous research. This buckling stress response surface is used as an objective function in the stacking sequence optimization.

Similarly, the response surface of thermal deformation with the lamination parameters was constructed from 100 selected runs of FEM analyses. Figure 6 shows

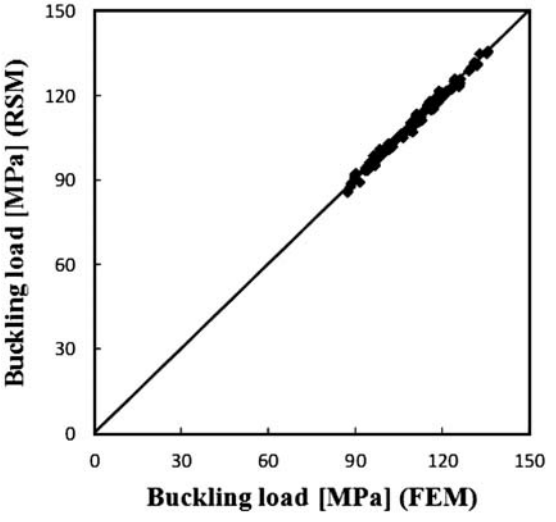

Figure 5. Estimations of response surface of buckling load using quadratic polynomial.

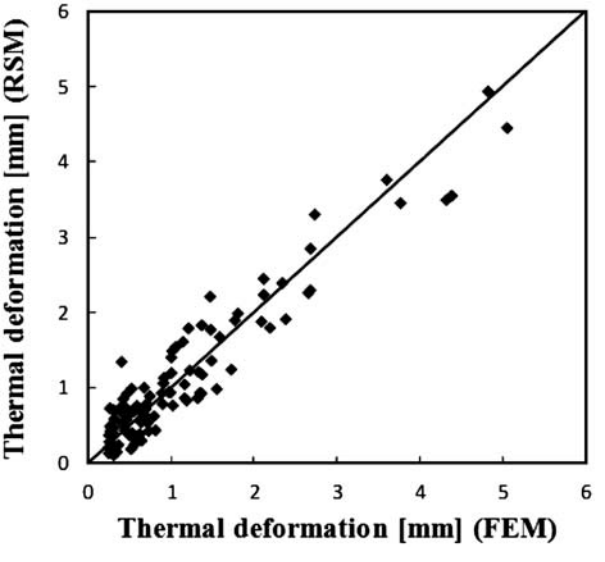

Figure 6. Estimations of response surface of thermal deformation using quadratic polynomial.

the evaluation results of the quadratic polynomial response surface of the lamination parameters. The abscissa is the maximum thermal deformation, obtained from FEM analyses. The ordinate is the estimation of the quadratic polynomial response surface. The obtained adjusted coefficient of determination R^2_{adj} is 0.88. The response surface of the thermal deformation is used to judge the satisfaction of the constraint. For the objective function, a small error of the response surface is acceptable because the candidate has a large objective function value. For the constraint, however, a small error is unacceptable. We consider the case where the laminate has a maximum buckling stress and is within the thermal deformation of 0.15 mm estimated from the response surfaces. When the constraint response surface has a small error and the actual thermal deformation is 0.151 mm, the optimal candidate laminate is rejected because of the violation of the constraint. The constraint response surface, therefore, must be exact. The $R^2_{adj} = 0.88$ is insufficient for the response surface of the constraint.

As shown in Equations (16)–(18), the linear thermal expansion coefficient of a symmetric composite laminate comprises of material properties and an in-plane lamination parameter. The relationship, however, is a complicated rational function. This means that the higher order polynomials are indispensable to obtaining the exact response surface. Higher order polynomials require many interaction terms and the increase in interaction terms require many FEM runs. To prevent the increase in FEM analyses runs, the linear thermal expansion coefficients of the laminated plate and stiffener were added to the response surface variables. Figure 7 shows the results of the response surface. The obtained adjusted coefficient of determination R^2_{adj} is 0.98. The R^2_{adj} is improved significantly by this slight increase in variables, although the quadratic polynomial is adopted in the response surface.

Figures 8 and 9, show results of the response surface of the mode classification method for each mode. As mentioned previously, the entire laminate can be classified into two modes, a type A and B saddle. The classification is based on the comparison of linear thermal expansion coefficient of the x-direction of the laminated plate and

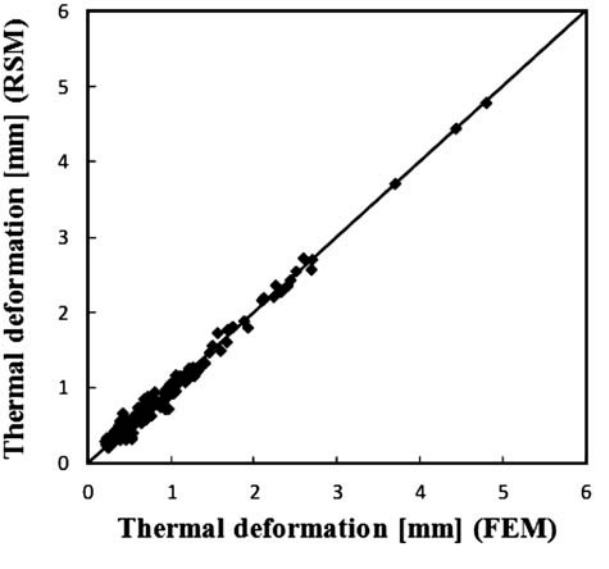

Figure 7. Estimations of response surface of thermal deformation using quadratic polynomial with linear thermal expansion coefficients.

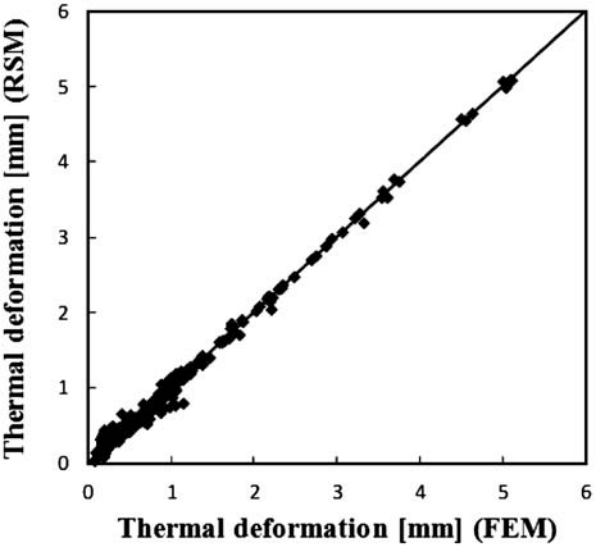

Figure 8. Estimations of response surface of thermal deformation using quadratic polynomial with mode classification for type A.

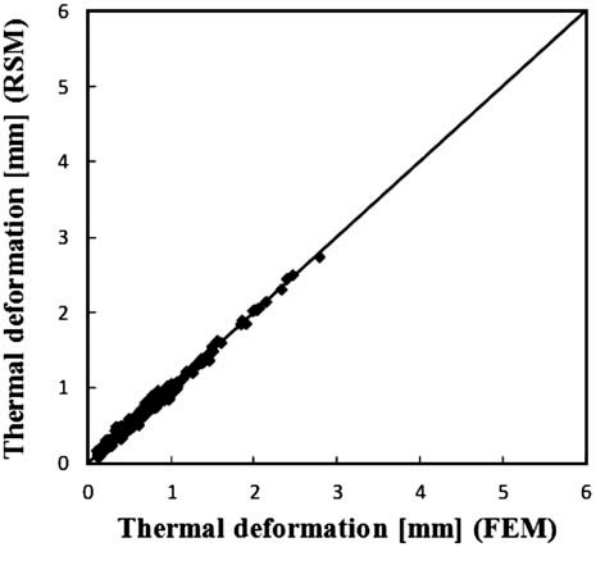

Figure 9. Estimations of response surface of thermal deformation using quadratic polynomial with mode classification for type B.

stiffener after the classification; D-optimal laminates were selected and 250 runs of FEM analyses were performed to make each response surface. In total, 500 FEM analyses runs were required. The obtained adjusted coefficient of determination R^2_{adj} was 0.99. The response surface of the mode classification provided significantly improved estimations. As the R^2_{adj} of the mode classification method was higher than the thermal coefficient response surface, the mode classification response surface was adopted here for the optimization constraint.

5.2. Optimization results

As mentioned in the previous section, the normal response surface of the buckling stress was adopted as an objective function and the mode classification response surface was used for evaluation of the constraint. A stacking sequence optimization was performed using the entire search method to prevent the limitation of the optimizer algorithm. As a result, the obtained optimal plate was $[0/90_3]$s and stiffener was $[90_3/\pm45/(90/0_4)_2]$s. After obtaining the provisional optimized result, FEM analysis was performed to confirm the optimization. According to the FEM analysis, the provisional optimal results violated the thermal deformation constraint with a deformation of 0.29 mm. This indicates that the mode classification response surface was slightly too low.

In this study, therefore, a zooming response surface method was adopted. To define the zoomed area, a Euclidean distance in the lamination parameter coordinates was used to judge the near optimal area. The distance was selected to be 2.8, because almost one-third of the entire design space was included in the area.[22] Although the zoomed response surface had a similar R^2_{adj} of 0.99, the estimation around the provisional optimal result was more exact than the entire area response surface. The result obtained was $[(0/90)_2]$s for the plate and $[(45/-45)_3/90_2/45/-45/90/0_4]$s for the stiffener.

To investigate the optimization, adjacent laminates were investigated. Figure 10 shows the adjacent laminates around the optimal laminate in the in-plane lamination parameter space.[22] There were eight adjacent laminates at the maximum. Of course, when the optimal laminate had no 45°-ply or −45°-ply, the number (1), (2), and (8) exchanges could not be performed. This means that the optimal laminate had only five adjacent laminates. For the out-of-plane lamination parameters, there were six adjacent laminates as shown in Figure 11.[22] In Table 2, the component is the target for investigation of adjacent laminates. The adjacent parameter corresponds to the adjacent lamination parameters that are focused on. Therefore, for example, 'plate/V' means the stiffener is fixed and the adjacent plate laminates are investigated. Thus, the stacking sequence is the laminate of the plate in this case. Thermal deformation and buckling stress were calculated using FEM analyses.

FEM analysis of the optimal laminate result shows that the thermal deformation is 0.07 mm and the buckling stress is 116.1 MPa. This satisfies the thermal deformation constraint. The laminates adjacent to the optimal laminate are shown in Table 2. From Table 2, a superior to provisional optimal laminate exists. Laminate 'I' has a 161.7 MPa buckling stress. The difference in buckling stress is, however, only 0.53% higher than the provisional optimal structure. This means that the zoomed response surface provides

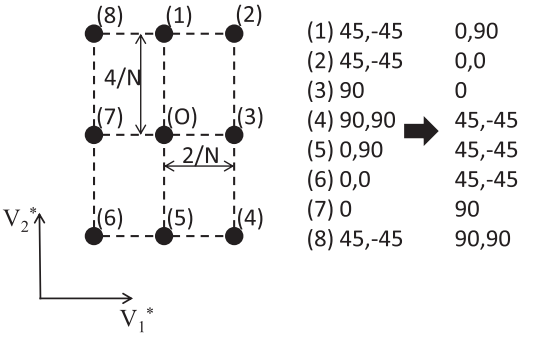

Figure 10. Adjacent laminates in in-plane lamination parameter space.[22]

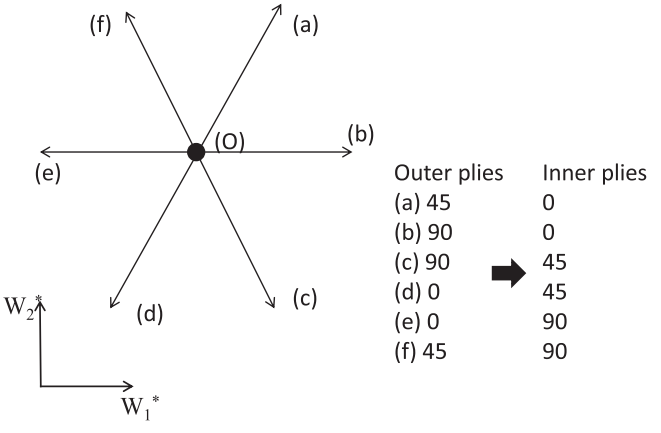

Figure 11. Adjacent laminates in out-of-plane lamination parameter space (45 means + 45 or −45).[22]

Table 2. Adjacent laminates to the optimal result (plate: [(0/90)2]s, stiffener: [(45/−45)3/902/45/−45/90/04]s).

Component/adjacent parameter	Stacking sequence	Thermal deformation (mm)	Buckling stress (MPa)
Plate/V	A:$[0/90/0_2]_S$	0.305	131.7
	B:$[0/45/0/45]_S$	0.753	119.6
	C:$[0/90/\pm45]_S$	0.048	115.2
	D:$[45/90/-45/90]_S$	0.480	91.5
	E:$[0/90_3]_S$	0.327	115.8
Plate/W	F:$[0_2/90_2]_S$	0.067	113.7
	G:$[0/90_2/0]_S$	0.063	116.2
Stiffener/V	H:$[(\pm45)_3/90_2/0/90_2/0_4]_S$	0.063	116.3
	I:$[(\pm45)_3/90_2/0_2/90/0_4]_S$	0.120	116.7
	J:$[(\pm45)_3/90/0/\pm45/90/0_4]_S$	0.142	116.4
	K:$[(\pm45)_3/90/(\pm45)_2/0_4]_S$	0.179	116.2
	L:$[(\pm45)_3/90_2/\pm45/45/0_3/-45]_S$	0.094	115.6
	M:$[(\pm45)_3/90_2/\pm45/90/0_2/\pm45]_S$	0.112	115.0
	O:$[(\pm45)_3/90_2/\pm45/90/0_3/90]_S$	0.103	115.4
	P:$[(\pm45)_3/90_2/\pm45/90/0_4]_S$	0.082	116.0
Stiffener/W	Q:$[(\pm45)_3/90_2/45/90/-45/0_4]_S$	0.072	116.1
	R:$[(\pm45)_3/90/45/90/-45/0_4]_S$	0.070	116.0
	S:$[(\pm45)_3/90_2/45/0/90/-45/0_3]_S$	0.069	116.0
	T:$[(\pm45)_3/90_2/\pm45/0/90/0_3]_S$	0.066	116.0

a sufficiently precise approximation for optimization of the stacking sequence with a constraint in thermal deformation.

6. Concluding remarks

Stacking sequence optimizations were dealt with, in this study. The response surface of the thermal deformation was focused on as a constraint of the stacking sequence

optimization. A blade-stiffened composite plate was adopted as target structure. Three types of response surfaces were proposed. The mode classification response surface provided the best fit to the thermal deformation of the stiffened composite structures. Two saddle type deformation modes were found and two response surfaces were made on the basis of the deformation modes. As a result, the zoomed response surfaces provided practically optimal stacking sequences with the constraint of thermal deformation.

References

[1] Miki M. Design of laminated fibrous composite plates with required flexural stiffness. ASTM STP. 1985;846:387–400.
[2] Fukunaga H, Vanderplaats G. Stiffness design method of symmetric laminate using lamination parameters. AIAA J. 1992;30:2791–2795.
[3] Le Riche R, Haftka RT. Optimization of laminate stacking sequence for buckling load maximization by genetic algorithm. AIAA J. 1993;31:951–956.
[4] Nagendra S, Jestina D, Gürdal Z, Haftka RT, Watson LT. Improved genetic algorithm for the design of stiffened composite panels. Comput. Struct. 1996;58:543–555.
[5] Liu B, Haftka RT, Akgün M, Todoroki A. Permutation genetic algorithm for stacking sequence design of composite laminates. Comput. Methods Appl. Mech. Eng. 2000;186:357–372.
[6] Park JH, Hwang JH, Lee CS, Hwang W. Stacking sequence design of composite laminates for maximum strength using genetic algorithms. Compos. Struct. 2001;52:217–231.
[7] Soremekun G, Gürdal Z, Kassapoglou C, Toni D. Stacking sequence blending of multiple composite laminates using genetic algorithms. Compos. Struct. 2002;56:53–62.
[8] Cho MH, Rhee SY. Layup optimization considering free-edge strength and bounded uncertainty of material properties. AIAA J. 2003;41:2274–2282.
[9] Kang JH, Kim CG. Minimum-weight design of compressively loaded composite plates and stiffened panels for postbuckling strength by genetic algorithm. Compos. Struct. 2005;69:239–246.
[10] Herencia JE, Weaver Paul M, Friswell MI. Optimization of long anisotropic laminated fiber composite panels with T-shaped stiffeners. AIAA J. 2007;45:2497–2509.
[11] Liu X, Bai Z, Shuang Y, Zhou C, Shao J. Optimization design for laminated composite structure based on Kriging Model. Appl. Mech. Mater. 2012;217–219:179–183.
[12] Narita Y. Layerwise optimization for the maximum fundamental frequency of laminated composite plates. J. Sound Vib. 2003;263:1005–1016.
[13] Terada Y, Todoroki A, Shimamura Y. Stacking sequence optimizations using fractal branch and bound method for laminated composites. JSME Int. J., Ser. A. 2001;44:490–498.
[14] Todoroki A, Terada Y. Improved fractal branch and bound method for stacking sequence optimizations of laminated composite stiffener. AIAA J. 2001;42:141–148.
[15] Sekishiro M, Todoroki A. Extended fractal branch and bound method for optimization of multiple stacking sequences of stiffened composite panel. Adv. Compos. Mater. 2006;15:341–356.
[16] Hirano Y, Todoroki A. Stacking sequence optimizations for composite laminates using fractal branch and bound method (Application for supersonic panel flutter problem with buckling load condition). Adv. Compos. Mater. 2004;13:89–107.
[17] Todoroki A, Sekishiro M. Modified efficient global optimization for a hat-stiffened composite panel with buckling constraint. AIAA J. 2008;46:2257–2264.
[18] Todoroki A, Sekishiro M. Two-level optimization of dimensions and stacking sequences for hat-stiffened composite panel. J. Comp. Sci. Technol., JSME. 2007;1:22–33.
[19] Todoroki A, Shinoda T, Mizutani Y, Matsuzaki R. New surrogate model to predict fracture of laminated CFRP for structural optimization. J. Comp. Sci. Technol., JSME. 2011;5:26–37.
[20] Todoroki A, Sekishiro M. Optimization of blade stiffened composite panel under buckling and strength constraints. J. Comp. Sci. Technol., JSME. 2008;2:234–245.
[21] Todoroki A, Ishikawa T. Design of experiments for stacking sequence optimizations with genetic algorithm using response surface approximation. Compos. Struct. 2004;64:349–357.
[22] Todoroki A, Sasai M. Stacking sequence optimizations using GA with zoomed response surface on lamination parameters. Adv. Compos. Mater. 2002;11:299–318.